Ionics (2019) 25:3523–3529
https://doi.org/10.1007/s11581-019-02923-8

ORIGINAL PAPER

The effect of anode structure on the performance of NiO-$BaZr_{0.1}Ce_{0.7}Y_{0.2}O_{3-\delta}$ supported ceria-based solid oxide fuel cells

Yusen Wu[1] · Zheng Gong[1] · Jie Hou[1] · Lina Miao[1] · Haidi Tang[1] · Wei Liu[1,2]

Received: 13 January 2019 / Revised: 31 January 2019 / Accepted: 7 February 2019 / Published online: 21 February 2019

Abstract

In this work, two asymmetric NiO-$BaZr_{0.1}Ce_{0.7}Y_{0.2}O_{3-\delta}$ (NiO-BZCY) anode substrates were prepared via the phase-inversion tape casting method for $Ce_{0.8}Sm_{0.2}O_{2-\delta}$ (SDC)-based solid oxide fuel cells. The results showed that the anode support structure significantly influenced the electrochemical properties of the cells. The cell supported on the anode substrate consisted of a finger-like layer and a sponge-like layer outputs highest electrochemical performance with a maximum power density of 823 mW cm^{-2} at 650 °C and shows great superiority over the cell fabricated by a typical dry-pressing method. The excellent performances demonstrate that the phase-inversion tape casting technique is a good strategy in fabricating anode supports for SOFCs, and the anode structure with the relatively dense sponge-like layer as top surface is optimal to construct the complete cell.

Keywords Anode structure · Phase-inversion tape casting · Doped ceria · Electron-blocking layer · Open-circuit voltage

Introduction

Solid oxide fuel cell (SOFC), as an efficient and environmentally friendly energy conversion system, has attracted more and more attention in the past few decades [1–6]. With the development of SOFC, lowing operating temperature has become a central branch of research because it can resolve or relieve the several problems that are caused by high operating temperature including high fabrication and operating cost, and inferior long-term stability. However, the electrochemical performance of fuel cells will decrease significantly with decreasing operating temperature due to the thermal activation nature of the processes in these components. In order to obtain high performance at reduced temperatures, developing and using electrolyte materials with high ionic conductivity is critical [7, 8]. Therefore, doped ceria has absorbed wide concern and is used frequently as electrolyte since it shows high ionic conductivity in the middle-low temperatures [9].

Nevertheless, the Ce^{4+}/Ce^{3+} redox reaction occurs in reducing atmospheres under the fuel cell operating condition, leading to obvious internal short behavior in doped ceria. Such internal short circuit significantly decreases both the open-circuit voltages (OCVs) and the working efficiency of SOFCs [10–12], which severely limits their popularization and application. Recently, Sun et al. [13] proposed a simple and effective strategy to prevent doped ceria (DCO) from reduction via substituting NiO-SDC with NiO-BZCY as the anode. By this approach, an electron blocking layer was formed at anode/electrolyte interface during the co-sintering process of half cells where the Ba elements diffused from the anode to react with SDC electrolyte. Although the OCVs improved significantly, the power performance was still not satisfactory as compared with traditional DCO-based fuel cells, especially at low operating temperature [14, 15]. In addition, the dry-press process is a small-scale technique unfitting for mass production, and the fabricated anodes usually have a tortuous and irregular pore microstructure, which will slow the gas exchange between fuel gases and by-products.

Phase-inversion tape casting as a large-scale preparation technique has been widely used in the manufacture of SOFC anodes in the past several years [4, 16–18]. In this method,

✉ Wei Liu
wliu@ustc.edu.cn

[1] CAS Key Laboratory of Materials for Energy Conversion & Collaborative Innovation Center of Suzhou Nano Science and Technology, University of Science and Technology of China, Hefei 230026, People's Republic of China

[2] Key Laboratory of Materials Physics, Institute of Solid State Physics, Chinese Academy of Sciences, Hefei 230031, People's Republic of China

ceramic powder slurry in organic polymer solution is cast on a temporary substrate and transferred into a water bath for curing. In the water bath, the organic polymer solution separates into a polymer-lean and a polymer-rich phases by the exchange of organic solvent with water. Due to the occurrence of the polymer-rich phases, the slurry is solidified into a green tape. Since the phase separation rate decreases along the thickness direction, the prepared anode is characterized by a three-layered structure including a few micrometers thick relatively dense skin layer at the top, a few hundred micrometers thick highly porous finger-like layer in the middle, and a few ten micrometers thick relatively dense sponge-like layer at the bottom [19]. These unique structures are retained after firing at elevated temperatures. The skin layer or sponge-like layer can be eliminated at sintering process by using graphite sacrificial layer, leaving straight open pores in finger-like layer exposed to the gas phase; this is advantageous to the fuel gas and by-product transport and consequently decreasing the concentration polarization [20]. Therefore, it can be expected that NiO-BZCY anode-supported doped ceria-based SOFC with high power density and high OCV can be achieved by using improved phase-inversion tape casting.

In this work, two kinds of NiO-BZCY anode structures were fabricated by adjusting the position of graphite sacrificial layer. The SDC electrolyte and $Sm_{0.5}Sr_{0.5}Co_{3-\delta}$ (SSC)-SDC cathode layer were prepared by drop-coating and screen-printing methods, respectively. The influence of the anode structure on the electrochemical properties of the SOFC with a configuration of NiO-BZCY anode substrate | NiO-BZCY anode functional layer | SDC electrolyte membrane | SSC-SDC cathode layer was evaluated.

Experimental

SDC, SSC, and NiO-BZCY powders with a weight ratio of 65:35 were all prepared by a citrate-nitrate gel combustion method [6, 21]. Take the NiO-BZCY as an example. Firstly, $Ni(NO_3)_2{\cdot}6H_2O$, $Ba(NO_3)_2$, $Zr(NO_3)_4{\cdot}5H_2O$, $Ce(NO_3)_3{\cdot}6H_2O$, and $Y(NO)_3{\cdot}6H_2O$ metal nitrates with stoichiometric ratio were dissolved in the deionized water. Then, citric acid with a mole ratio of metal ions to citric acid at 1:1.5 was added to the solution under stirring. Subsequently, $NH_3{\cdot}H_2O$ was used to adjust the pH value of the solution to about 7. The solution was heated until a sticky gel was formed, and the gel was further heated to combustion by an electric furnace. The as-prepared NiO-BZCY was calcined at 1000 °C for 3 h to obtain a pure phase.

The phase-inversion tape casting was used to manufacture the asymmetric NiO-BZCY anode support substrate, and the details of the phase-inversion process were referred to in recent reports [16, 22]. Two different anode structures were obtained by adjusting the position of the graphite and the NiO-BZCY. The thickness was controlled by adjusting the blade clearance. The green tape was punched into pellets about 16 mm in diameter and then pre-sintered at 1000 °C for 2 h to eliminate the graphite layer. The SDC electrolyte membrane and anode functional layer (AFL) were prepared by the drop-coating method on the anode substrate surface and then co-fired at 1400 °C for 5 h [23, 24]. As a comparison, NiO-BZCY (65:35 wt.%) anode substrates with 20 wt.% starch as the pore-forming agent, NiO-BZCY AFL and SDC electrolyte membrane were fabricated by the dry-pressing method under 300 MPa. After that, the green cell was co-fired at 1400 °C for 5 h. The SSC-SDC (6:4) powders were added to the appropriate ethylcellulose-terpineol binder, which were ground to form a cathode slurry. The cathode slurry was then coated on the SDC electrolyte membrane with the screen printing method, and a single cell was formed by co-fired at 950 °C for 2 h.

To evaluate the gas permeability and porosity of the Ni-BZCY anodes, the anodes were heat-treated under the same conditions with as the assembling complete cells, and then reduced at 800 °C for 5 h in the humidified H_2 (~3% H_2O) to form Ni-BZCY anode substrates. The gas permeability of the samples was measured using a homemade setup described in [25, 26]. The porosities were measured using the Archimedes method [27].

The microstructure and morphology of the single cells were investigated by a scanning electron microscopy (SEM; JEOL JSM-6700F). In the homemade test system, single cells were tested with a flow rate of 40 mL min^{-1} humidified H_2 (~3% H_2O) as the feed gas. The current–voltage curves were measured by DC Electronic Load (IT8511). The electrochemical impedance spectra (EIS) of the cells were measured by the impedance analyzer (CHI604B) from 10^5 to 10^{-1} Hz under OCV.

Table 1 Fabrication method and sintering temperature of cells I to III

Cell	Anode fabrication method	Electrolyte fabrication method	Cathode fabrication method	Sintering temperature
I	Phase-inversion tape casting removed the skin layer	Drop-coating	Screen-printing	1400 °C
II	Phase-inversion tape casting removed the sponge-like layer	Drop-coating	Screen-printing	1400 °C
III	Dry-pressing	Dry-pressing	Screen-printing	1400 °C

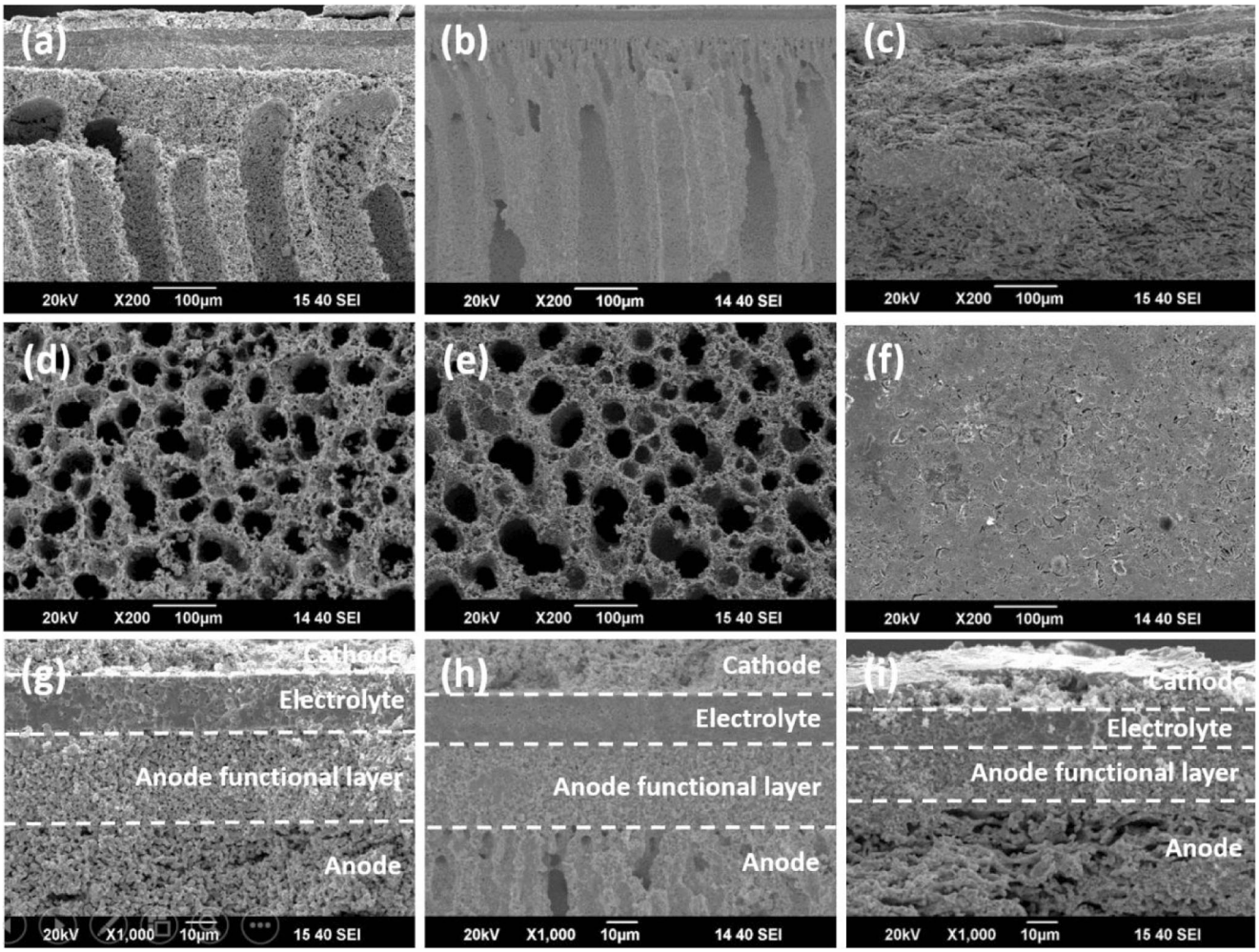

Fig. 1 Cross-sectional morphology of **a**, **g** cell I, **b**, **i** cell II, and **c**, **i** cell III. The SEM images of the anode bottom surface of **d** cell I, **e** cell II, and **f** cell III

Result and discussion

It has been demonstrated that the electrochemical properties of SOFC are closely related to the microstructure of anode electrode [28, 29]. To evaluate the NiO-BZCY anode structure on the performance of the SDC-based SOFC, three kinds of fuel cells were prepared, corresponding to cell I, cell II, and cell III, which have different anode microstructures. Table 1

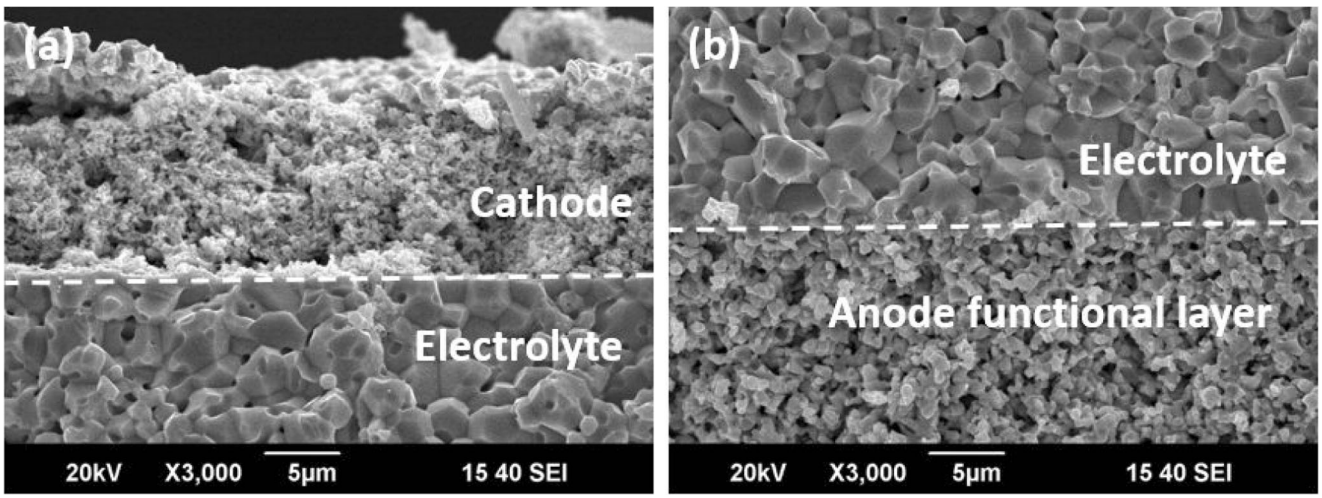

Fig. 2 Cross-sectional SEM images of **a** the interface between cathode and electrolyte and **b** the interface between electrolyte and AFL of the cell I

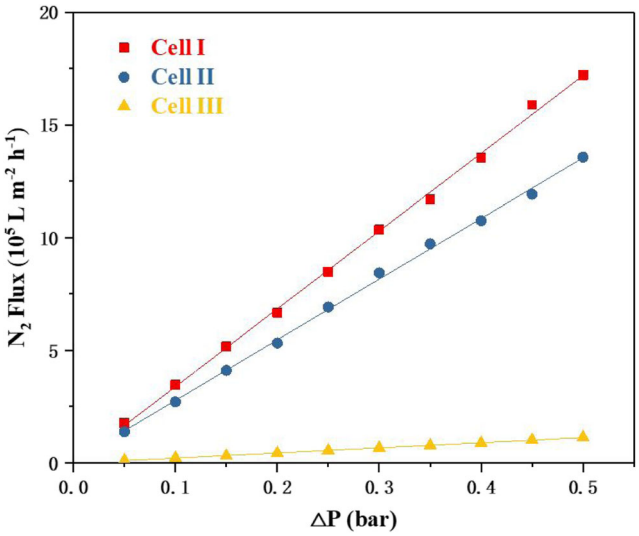

Fig. 3 The anode gas permeability of cells I to III

summarizes the fabrication parameters of the cells. The SEM images of the fuel cells with different anode support microstructure after testing are shown in Fig. 1 for (a, d, and g) cell I, (b, e, and h) cell II, and (c, f, and i) cell III, respectively. One can see that the anode supports of cells I and II fabricated by the phase-inversion tape casting method contain typical large finger-like pores (Fig. 1a, b). There is no doubt that this structure is benefit to transport fuels and by-products that formed during operation of fuel cell. In contrast, the anode support of cell III fabricated by a conventional dry-pressing method only has small tortuous and irregular pore microstructure (Fig. 1c). The total porosity of the reduced anode was measured by Archimedes method. It was found that the anodes prepared by phase-inversion tape casting method had higher porosity. The total porosities were 69.7%, 72.4%, and 48.7% for the cell I, cell II, and cell III anodes, respectively. It should be noted that the anode support of cell I consists of an asymmetric two-layered structure including thin, relatively dense sponge-like layer and thick finger-like layer, while the anode support of cell II consists of thin, relatively dense skin layer and thick finger-like layer. Compared with the skin layer, relatively dense sponge-like layer in the anode support of cell I possessed smaller and uniform pores, which will enlarge three-phase boundaries (TPBs) and provide more sufficient

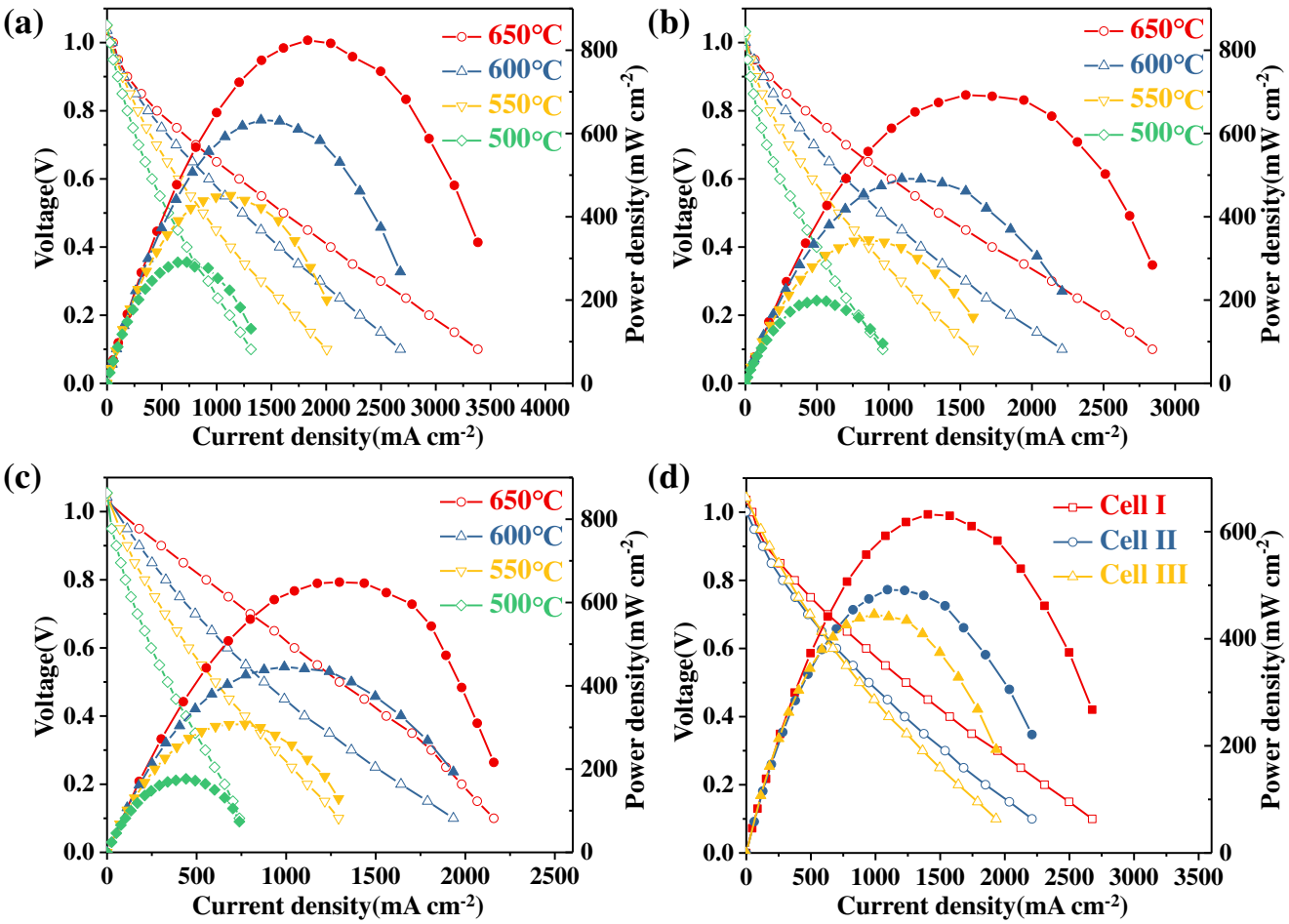

Fig. 4 I-V and I-P curves of **a** cell I, **b** cell II, **c** cell III, and **d** the cells with different anode structure at 600 °C measured in a wet hydrogen atmosphere at 500–650 °C

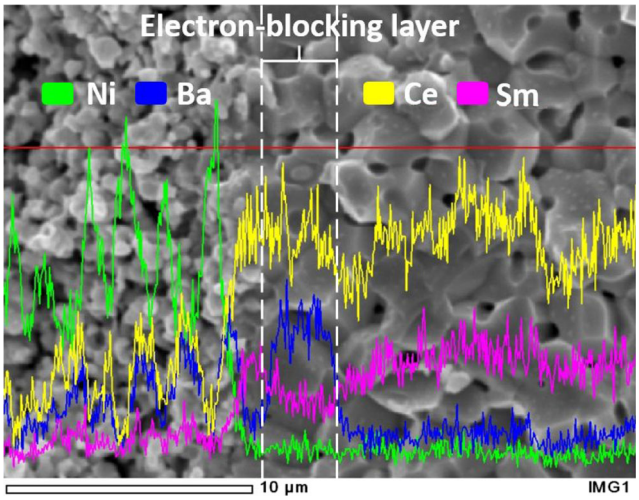

Fig. 5 SEM-EDS analysis of the interface between SDC electrolyte membrane and AFL of the cell I sintered at 1400 °C for 5 h after testing

catalytic activity sites for electrochemical reactions. Figure 1d–f shows the bottom surface SEM micrographs of the anode supports. One can see that the pores with a few ten micrometers in diameter in finger-like layer of cells I and II were completely open to air. Besides, all the electrolyte membranes of the fuel cells with different anode microstructure are fully dense, crack-free and well contacted with electrodes, which can be observed from Fig. 1g–i.

It has been reported that macropores at the electrolyte/anode substrate interface decreased the contact between the electrolyte and the anode substrate, reducing the TPB length, consequently, impairing the fuel cell performance. In contrast, the anode functional layers with low porosity have more uniform and smaller pores, which can optimize the microstructure and provide more catalytic active sites for electrochemical reaction [30, 31]. Therefore, an anode functional layer was fabricated to optimize the cell's performance. Figure 2a, b is an enlarged view of the electrolyte/electrode interface for the cell I, which can further prove the firm combination of the layers.

To achieve high-performance anode-supported SOFCs, the anode substrates should have high porosity for fast mass transport [26, 32]. The gas permeability of the reduced anodes was determined and summarized in Fig. 3. It was found that the anode substrates of cell I and cell II prepared by the phase-inversion tape casting method showed excellent gas permeability. The calculated N_2 permeability was 34.5, 26.9, and 2.3×10^5 $Lm^{-2}h^{-1}bar^{-1}$ for cell I, cell II, and cell III anodes, respectively. One can see that the gas permeability of cell I and cell II anode were one order of magnitude higher than the cell III. In addition, the gas permeability of cell I is superior to that of cell II. Therefore, it is expected that there should be little resistance to gas transfer during the operation for cell I, and correspondingly enhancing the electrochemical performance. Besides, the anode of cell I with sponge layer has small and uniform pores, which will expand TPBs and provide more sufficient catalytic activity sites for electrochemical reactions [33]. Therefore, the anode structure with the relatively dense sponge-like layer as top surface may be optimal to construct the complete cell.

The I-V and I-P curves of different anode-supported structures fuel cells are presented in Fig. 4a–c for cells I, II, and III. The I-V and I-P curves of the cells I, II, and III tested at 600 °C are plotted in Fig. 4d for comparison. The maximum power densities (MPDs) of the cells I, II, and III are 632, 491, and 445 mW cm^{-2} at 600 °C, respectively. As can be seen, the performances of both cells I and II with anode supports prepared by the phase-inversion tape casting are superior to that of the cell III with anode support prepared by dry-pressing, demonstrating that the phase-inversion tape casting technique is a good method in fabricating anode supports for SOFCs. Besides, the cell I with the relatively dense sponge-like layer as the top surface outputs highest power densities, and the MPDs are 823 mW cm^{-2} at 650 °C, 632 mW cm^{-2} at 600 °C, 451 mW cm^{-2} at 550 °C,

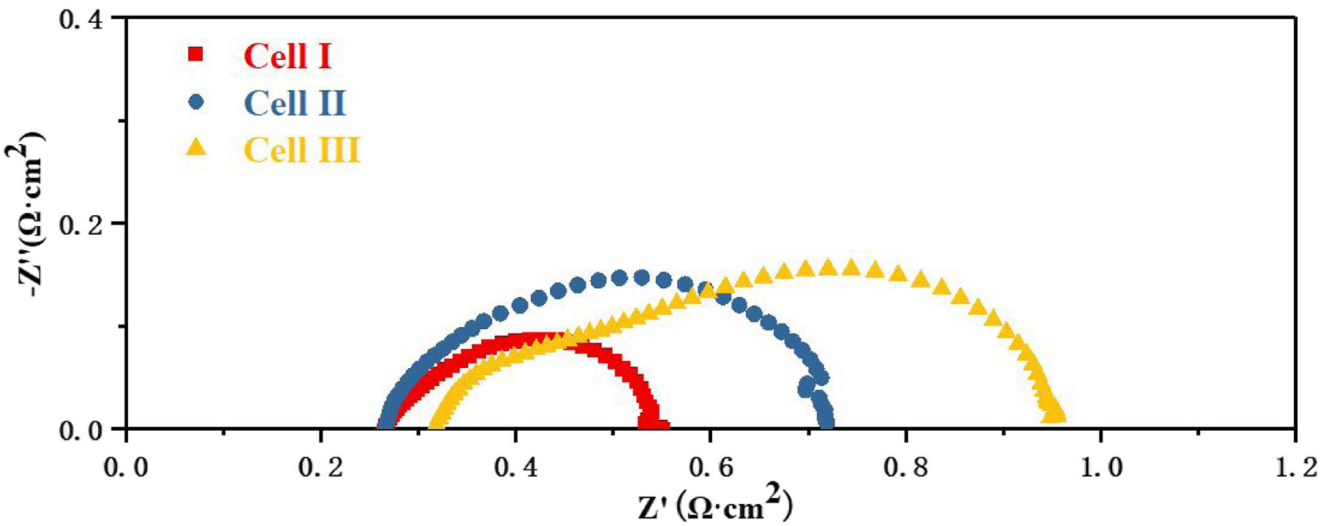

Fig. 6 EIS of the cells I, II, and III measured at 600 °C under open-circuit conditions

Table 2 The ohmic resistance, polarization resistance, and total resistance from the EIS under open-circuit conditions and corresponding operating temperature

Cell	I			II			III		
T (°C)	R_o (Ωcm^2)	R_p (Ωcm^2)	R_t (Ωcm^2)	R_o (Ωcm^2)	R_p (Ωcm^2)	R_t (Ωcm^2)	R_o (Ωcm^2)	R_p (Ωcm^2)	R_t (Ωcm^2)
650	0.22	0.14	0.36	0.21	0.22	0.43	0.21	0.23	0.44
600	0.26	0.28	0.54	0.26	0.46	0.72	0.31	0.64	0.95
550	0.34	0.67	1.01	0.33	1.00	1.33	0.44	1.47	1.91
500	0.47	1.24	1.71	0.45	1.86	2.31	0.69	3.92	4.61

and 291 mW cm^{-2} at 500 °C. As a comparison, the cell II with relatively dense skin layer as the top surface only achieved 692 mW cm^{-2} at 650 °C, 491 mW cm^{-2} at 600 °C, 344 mW cm^{-2} at 550 °C, and 198 mW cm^{-2} at 500 °C. The results indicated that sponge-like layer should be more suitable for the top surface to construct the single cell. The discrepancy of performance may attribute to different microstructure between the sponge-like layer and skin layer shown in Fig. 1.

It is important to note that the corresponding OCVs of the cell I reached 1.01 V at 650 °C, 1.036 V at 600 °C, 1.043 V at 550 °C, and 1.052 V at 500 °C, which are obviously higher than those of the typical DCO-based SOFCs [2, 34]. The improved OCVs indicate that the electronic current is effectively blocked through the SDC electrolyte. The electron blocking layer is formed in situ via the reaction between diffused Ba elements, and SDC electrolyte was supposed to the reason of the improved OCV [12, 35]. To confirm the electron blocking layer, the AFL/electrolyte interface was measured by the SEM-EDS analysis and shown in Fig. 5. It can be seen that there is an obvious diffusion layer of Ba element about 2 μm in thickness. The results match well with previous reports [13].

Figure 6 shows the typical EIS of the cells measured at 600 °C under open-circuit conditions. Both polarization resistance (R_p) and ohmic resistance (R_o) can be obtained from EIS [36, 37]. The R_o of the cells I, II, and III is calculated to be 0.26, 0.26, and 0.31 Ωcm^2, while R_p is 0.28, 0.46, and 0.64 Ωcm^2 at 600 °C, respectively. The R_o and R_p of the cells I, II, and III at other tested temperatures are shown in Table 2. It can be found that the cell I shows the lowest R_p, which is well accorded with the cell performance. Given all the cells have the same anode, electrolyte, and cathode materials, the different R_p should be ascribed to the different anode microstructure, which sensitively affects the amount of TPBs as well as the fuel gas and by-product transport [28]. The EIS results further demonstrated that the anode structure with the relatively dense sponge-like layer as top surface derived from phase inversion is favorable for the SOFCs.

Conclusions

The finger-like porous layer formed by phase-inversion tape casting method can allow for rapid gas phase transportation and thus greatly reduce the concentration polarization. This work compared the effect of the anode support structures prepared by removing the skin layer or sponge-like layer on the cell performance. The cell supported by an anode substrate consisting of the sponge-like layer and finger-like layer exhibits better electrochemical performance, which is due to the finger-like porous structure and the microstructure of sponge-like layer with small and uniform pores by reducing the concentration polarization and enlarging TPBs. The MPDs of the cell achieved 823 mW cm^{-2} at 650 °C, 632 mW cm^{-2} at 600 °C, 451 mW cm^{-2} at 550 °C, and 291 mW cm^{-2} at 500 °C. These results reveal that the anode support fabricated by the modified phase-inversion tape casting technique is a good alternative for SOFCs.

Funding This work was supported by the National Science Foundation of China (Grant Nos. 21676261 and U1632131).

References

1. Iwahara H, Yajima T, Hibino T, Ozaki K, Suzuki H (1993) Protonic conduction in calcium, strontium and barium zirconates. Solid State Ionics 61:65–69
2. Shao Z, Haile SM (2004) A high-performance cathode for the next generation of solid-oxide fuel cells. Nature 431:170–173
3. Atkinson A, Barnett S, Gorte RJ, Irvine JTS, Mcevoy AJ, Mogensen M, Singhal SC, Vohs J (2004) Advanced anodes for high-temperature fuel cells. Nat Mater 3:17–27
4. Suzuki T, Hasan Z, Funahashi Y, Yamaguchi T, Fujishiro Y, Awano M (2009) Impact of anode microstructure on solid oxide fuel cells. Science 325:852–855
5. Yang L, Wang S, Blinn K, Liu M, Liu Z, Cheng Z, Liu M (2009) Enhanced sulfur and coking tolerance of a mixed ion conductor for SOFCs: $BaZr_{0.1}Ce_{0.7}Y_{0.2-x}Yb_xO_{3-\delta}$. Science 326:126–129
6. Dai H, Da'as EH, Shafi SP, Wang H, Bi L (2018) Tailoring cathode composite boosts the performance of proton-conducting SOFCs fabricated by a one-step co-firing method. J Eur Ceram Soc 38: 2903–2908
7. Ren C, Gan Y, Lee M, Yang C, He F, Jiang Y, Dong G, Green RD, Xue X (2016) Fabrication and characterization of high performance intermediate temperature micro-tubular solid oxide fuel cells. J Electrochem Soc 163:F1115–F1123

8. Bi L, Fabbri E, Sun Z, Traversa E (2011) A novel ionic diffusion strategy to fabricate high-performance anode-supported solid oxidefuel cells (SOFCs) with proton-conducting Y-doped $BaZrO_3$ films. Energy Environ Sci 4:409–412
9. Yang RJ, Lee MC, Chang JC, Lin TN, Chang YC, Kao WX, Lee LS, Cheng SW (2012) Fabrication and characterization of a $Sm_{0.2}Ce_{0.8}O_{1.9}$ electrolyte film by the spin-coating method for a low-temperature anode-supported solid oxide fuel cells. J Power Sources 206:111–118
10. Eguchi K, Setoguchi T, Inoue T, Arai H (1992) Electrical properties of ceria-based oxides and their application to solid oxide fuel cells. Solid State Ionics 52:165–172
11. Doshi R, Richards VL, Carter JD, Wang X, Krumpelt M (1999) Development of solid-oxide fuel cells that operate at 500°C. J Electrochem Soc 146:1273–1278
12. Gong Z, Sun W, Shan D, Wu Y, Liu W (2016) Tuning the thickness of Ba-containing "functional" layer toward high-performance ceria-based solid oxide fuel cells. ACS Appl Mater Interfaces 8:10835–10840
13. Sun W, Liu W (2012) A novel ceria-based solid oxide fuel cell free from internal short circuit. J Power Sources 217:114–119
14. Wachsman ED, Lee KT (2011) Lowering the temperature of solid oxide fuel cells. Science 334:935–939
15. Atkinson A (1997) Chemically-induced stresses in gadolinium-doped ceria solid oxide fuel cell electrolytes. Solid State Ionics 95:249–258
16. Huang H, Lin J, Wang Y, Wang S, Xia C, Chen C (2015) Facile one-step forming of NiO and yttrium-stabilized zirconia composite anodes with straight open pores for planar solid oxide fuel cell using phase-inversion tape casting method. J Power Sources 274:1114–1117
17. Han Z, Wang Y, Yang Z, Han M (2016) Electrochemical properties of tubular sofc based on a porous ceramic support fabricated by phase-inversion method. J Mater Sci Technol 32:681–686
18. Sun H, Chen Y, Yan R, Wei T, Zhang Y, Zhang Q, Bu Y, Liu M (2016) Anode-supported solid oxide fuel cells based on $Sm_{0.2}Ce_{0.8}O_{1.9}$ electrolyte fabricated by a phase-inversion and drop-coating process. Int J Hydrog Energy 41:10907–10913
19. Liu T, Wang Y, Zhang Y, Fang S, Lei L, Ren C, Chen F (2015) Steam electrolysis in a solid oxide electrolysis cell fabricated by the phase-inversion tape casting method. Electrochem Commun 61:106–109
20. Kingsbury BFK, Li K (2009) A morphological study of ceramic hollow fibre membranes. J Membr Sci 328:134–140
21. Sun W, Yan L, Shi Z, Zhu Z, Liu W (2010) Fabrication and performance of a proton-conducting solid oxide fuel cell based on a thin $BaZr_{0.8}Y_{0.2}O_{3-\delta}$ electrolyte membrane. J Power Sources 195: 4727–4730
22. Lin J, Miao G, Xia C, Chen C, Wang S, Zhan Z (2017) Optimization of anode structure for intermediate temperature solid oxide fuel cell via phase-inversion cotape casting. J Am Ceram Soc 100:3794–3800
23. Sun W, Shi Z, Liu M, Bi L, Liu W (2014) An easily sintered, chemically stable, barium zirconate-based proton conductor for high-performance proton-conducting solid oxide fuel cells. Adv Funct Mater 24:5695–5702
24. Ling Y, Chen J, Wang Z, Xia C, Peng R, Lu Y (2013) New ionic diffusion strategy to fabricate proton-conducting solid oxide fuel cells based on a stable $La_2Ce_2O_7$ electrolyte. Int J Hydrog Energy 38:7430–7437
25. Van de Graaf JM, Kapteijn F, Moulijn JA (1998) Methodological and operational aspects of permeation measurements on silicalite-1 membranes. J Membr Sci 144:87–104
26. Liu T, Ren C, Zhang Y, Wang Y, Lei L, Chen F (2017) Solvent effects on the morphology and performance of the anode substrates for solid oxide fuel cells. J Power Sources 363:304–310
27. Taylor RP, McClain ST, Berry J (1999) Uncertainty analysis of metal-casting porosity measurements using Archimedes' principle. Int J Cast Met Res 11:247–257
28. Liu T, Ren C, Fang S, Wang Y, Chen F (2014) Microstructure tailoring of the nickel oxide–yttria-stabilized zirconia hollow fibers toward high-performance microtubular solid oxide fuel cells. ACS Appl Mater Interfaces 6:18853–18860
29. Zhang B, Wu K, Peng K (2018) Fabrication and characterization of $Nd_{2-x}In_xCe_2O_7$ proton-conducting electrolytes for intermediate-temperature solid oxide fuel cells. J Power Sources 399:157–165
30. Chen X, Lin J, Sun L, Liu T, Wu J, Sheng Z, Wang Y (2019) Improvement of output performance of solid oxide fuel cell by optimizing the active anode functional layer. Electrochim Acta 298:112–120
31. Bi L, Fabbri E, Traversa E (2012) Effect of anode functional layer on the performance of proton-conducting solid oxide fuel cells (SOFCs). Electrochem Commun 16:37–40
32. Singhal SC, Kendall K (2003) High-temperature solid oxide fuel cells: fundamentals, design and applications. Elsevier, Oxford, pp 149–168
33. Lee KT, Yoon HS, Ahn JS, Wachsman ED (2012) Bimodally integrated anode functional layer for lower temperature solid oxide fuel cells. J Mater Chem 22:17113–17120
34. Zhang X, Robertson M, Yick S, Deĉes-Petit C, Styles E, Qu W, Xie Y, Hui R, Roller J, Kesler O, Maric R, Ghosh D (2006) $Sm_{0.5}Sr_{0.5}CoO_3$+$Sm_{0.2}Ce_{0.8}O_{1.9}$ composite cathode for cermet supported thin $Sm_{0.2}Ce_{0.8}O_{1.9}$ electrolyte SOFC operating below 600°C. J Power Sources 160:1211–1216
35. Sun W, Shi Z, Qian J, Wang Z, Liu W (2014) In-situ formed $Ce_{0.8}Sm_{0.2}O_{2-\delta}$@$Ba(Ce, Zr)_{1-x}(Sm, Y)_xO_{3-\delta}$ core/shell electron-blocking layer towards $Ce_{0.8}Sm_{0.2}O_{2-\delta}$-based solid oxide fuel cells with high open circuit voltages. Nano Energy 8:305–311
36. Bi L, Da'as EH, Shafi SP (2017) Proton-conducting solid oxide fuel cell (SOFC) with Y-doped $BaZrO_3$ electrolyte. Electrochem Commun 80:20–23
37. Bi L, Fabbri E, Traversa E (2018) Solid oxide fuel cells with proton-conducting $La_{0.99}Ca_{0.01}NbO_4$ electrolyte. Electrochim Acta 260: 748–754